Triplet Excited State Distortions in a Pyrazolate Bridged Platinum Dimer Measured by X-ray Transient Absorption Spectroscopy

12 AUTHORS, INCLUDING:

G. Jennings
Argonne National Laboratory
103 PUBLICATIONS   **3,135** CITATIONS

Alexander Soldatov
Southern Federal University
241 PUBLICATIONS   **1,818** CITATIONS

Arnold Rheingold
University of California, San Diego
2,176 PUBLICATIONS   **51,288** CITATIONS

Lin X. Chen
Northwestern University
416 PUBLICATIONS   **8,411** CITATIONS

Triplet Excited State Distortions in a Pyrazolate Bridged Platinum Dimer Measured by X-ray Transient Absorption Spectroscopy

Jenny V. Lockard,[†] Aaron A. Rachford,[‡,§] Grigory Smolentsev,[∥,⊥] Andrew B. Stickrath,[†] Xianghuai Wang,[‡] Xiaoyi Zhang,[#] Klaus Atenkoffer,[#] Guy Jennings,[#] Alexander Soldatov,[∥] Arnold L. Rheingold,[∇] Felix N. Castellano,*[,‡] and Lin X. Chen*[,†,○]

Chemical Sciences and Engineering Division and X-ray Sciences Division, Argonne National Laboratory, Argonne, Illinois 60439, United States, Department of Chemistry, Northwestern University, Evanston, Illinois 60208, United States, Department of Chemistry & Center for Photochemical Sciences, Bowling Green State University, Bowling Green, Ohio 43403, United States, Research Center for Nanoscale Structure of Matter, Southern Federal University, Sorge 5, Rostov-na-Donu, 344090 Russia, Department of Chemical Physics, Lund University, P.O. Box 124, SE-22100, Lund, Sweden, and Department of Chemistry, University of California, San Diego, La Jolla, California 92093, United States

The excited-state structure of a dinuclear platinum(II) complex with *tert*-butyl substituted pyrazolate bridging units, [Pt(ppy)(μ-^{t}Bu$_2$pz)]$_2$ (ppy = 2-phenylpyridine; ^{t}Bu$_2$pz = 3,5-di-*tert*-butylpyrazolate) is studied by X-ray transient absorption (XTA) spectroscopy to reveal the transient electronic and nuclear geometry. DFT calculations predict that the lowest energy triplet excited state, assigned to a metal−metal-to-ligand charge transfer (MMLCT) transition, has a contraction in the Pt−Pt distance. The Pt−Pt bond length and other structural parameters extracted from fitting the experimental XTA difference spectra from full multiple scattering (FMS) and multidimensional interpolation calculations indicates a metal−metal distance decrease by approximately 0.2 Å in the triplet excited state. The advantages and challenges of this approach in resolving dynamic transient structures of nonbonding or weak-bonding dinuclear metal complexes in solution are discussed.

Introduction

Correlating excited-state properties with its structural changes in response to an electron density shift due to photoexcitation has been a research frontier since intense X-ray pulses became available from the third generation synchrotron sources and from the fourth generation X-ray free electron lasers. The advent of time-resolved vibrational techniques enabled the interrogation of bond length and angle changes along excited state pathways by measuring changes in excited state force constants.[1−3] With the development of 2D spectroscopy[1,4,5] and the increased sophistication of ultrafast lasers, a more detailed understanding of molecular structural dynamics in excited states and along the photochemical pathways can be acquired. Still, vibrational spectroscopy methods represent an indirect way of measuring structural change and are commonly limited by ambiguities in vibrational mode assignments. An alternative and in many ways complementary approach to studying excited-state structural change is X-ray transient absorption spectroscopy (XTA).[6−8] This technique combines the pump−probe methodology commonly used in optical spectroscopy with X-ray absorption

spectroscopy (XAS). A laser pump pulse is employed to generate the excited state population and an X-ray probe pulse is used to interrogate the ensuing molecular electronic and structural changes. The structurally sensitive aspects of XAS are maintained, allowing the detection of small geometry changes (within 0.02 Å) between ground and excited states. XTA has been successfully used to study the excited state pathways of several metal-containing systems including exciplex formation,[9] photodissociation intermediates[8] and triplet excited state distortions of metalloporphyrins,[10] the metal-to-ligand-charge transfer (MLCT) state structures of photoactive Cu(I) complexes,[11] and excited state dynamics[12] and structure[13] of iron spin crossover complexes.

Photoactive bimetallic complexes in which metal−metal interaction is promoted by bridging ligand scaffolding have been explored both for practical applications such as photocatalysis[14,15] and light-emitting diodes[16,17] and as fundamental studies of electron transfer[18−20] and metal−metal interactions.[21,22] One of the most extensively studied of these bimetallic complexes is the dinuclear platinum(II) diphosphite complex, [Pt$_2$(pop)$_4$]$^{4−}$ [pop = pyrophosphate, (H$_2$P$_2$O$_5$)$^{2−}$].[23−25] Simple MO theory predicts a higher metal−metal bond order in the ^{3}A$_{2u}$(dσ)^2(dσ*)^1(pσ)^1 excited state compared to the ^{1}A$_{1g}$(dσ)^2(dσ*)^2 ground state due to depopulation of the dσ* antibonding orbital. Evidence abounds for this stronger excited state Pt−Pt interaction and has been provided by steady-state[24] and time-resolved[26] resonance Raman spectroscopies and low temperature electronic absorption and emission spectroscopies.[27,28] Microsecond-resolved XAFS studies of Pt$_2$(pop)$_4$ yielded the first direct evidence for the contraction of the Pt−Pt distance in the excited state.[29] Using

* Corresponding authors: lchen@anl.gov and castell@bgsu.edu.
† Chemical Sciences and Engineering Division, Argonne National Laboratory.
‡ Department of Chemistry & Center for Photochemical Sciences, Bowling Green State University.
§ Current address: The Dow Chemical Company, Analytical Sciences, 1897 Building, Midland, MI 48667, USA.
∥ Research Center for Nanoscale Structure of Matter, Southern Federal University.
⊥ Department of Chemical Physics, Lund University.
X-ray Sciences Division, Argonne National Laboratory.
∇ Department of Chemistry, University of California, San Diego.
○ Department of Chemistry Northwestern University.

Triplet Excited State Distortions

J. Phys. Chem. A, Vol. 114, No. 48, 2010 **12781**

SCHEME 1
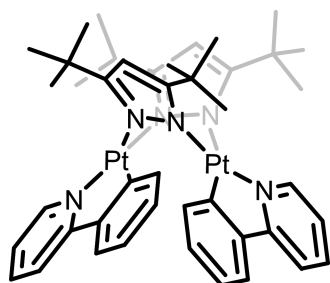
1

the pump−probe X-ray diffraction, Coppens et al. obtained from Pt₂(pop)₄ single crystals a shortening of the Pt−Pt bond by 0.28 Å in the triplet excited state.[30] Most recently, van der Veen et al. reported XTA measurements of Pt₂(pop)₄ in solution and claimed a reduction in Pt−Pt distance of 0.31 Å in the triplet excited state[31] and Christensen and co-workers reported time-resolved wide-angle X-ray scattering results of the same complex, which indicated a transient 0.24 Å contraction of the Pt−Pt distance in solution.[32]

In other types of dinuclear platinum complexes, the degree of Pt−Pt interactions has been modulated via modifying the bridging units. In a series of cyclometalated dinuclear platinum(II) complexes reported by Ma, Thompson, and co-workers, pyrazolate bridging ligands provide a scaffolding to permit ground-state metal−metal interactions while the degree of the interaction is tuned by the bulkiness of the groups at the 3- and 5- positions of the pyrazolate bridges.[17] The steric hindrance provided by these substituents forces the two Pt atoms closer together. When bulky *t*-Bu groups are used, the Pt−Pt distance is 2.83 Å as revealed by the crystal structure. This relatively short Pt−Pt distance leads to strong metal−metal interactions. A similar MO picture is used to predict the excited state Pt−Pt bond length change as in the Pt₂(pop)₄ system. The lowest energy triplet state in the cyclometalated dimer is assigned as a metal−metal-to-ligand charge transfer (MMLCT) arising from the transition from the dσ* orbital to π* orbital on one of the 2-(2,4-difluorophenyl)pyridine (F₂ppy) ligands. Transient depopulation of the σ* antibonding orbital predicts a stronger Pt−Pt interaction and thus shorter metal−metal bond distance. Indeed, DFT calculations have shown that the Pt−Pt distance in the optimized geometry for the lowest energy triplet state is 0.3 Å shorter than that of the singlet ground state.[33]

In this article, we present the XTA results measured on a similar dinuclear platinum(II) complex with *t*-Bu substituted pyrazolate bridging units, [Pt(ppy)(μ-ᵗBu₂pz)]₂ (**1**),[34] shown in Scheme 1. The XTA spectra exhibit the most pronounced changes in the XANES region. Extracting structural information from XANES spectra has been a challenge due to complications from multiple scattering effects intertwined with single scattering as well as the absorption from state to state transitions. Recently, a XANES analysis of the PtPOP anion has been reported with semiquantitative results that support the Pt−Pt distance change determined by more traditional EXAFS analysis.[35] A relatively new analysis technique based on a multidimensional interpolation approximation (MIA) method in combination with full multiple scattering (FMS) calculations has been shown to yield quantitative structural information from fitting solely the XANES spectra.[36,37] In this work, changes observed in the XANES region of the XTA spectra of **1** are fit using this analysis method. These difference spectrum calculations reveal the

geometry changes associated with the ³MMLCT excited state of **1** and are compared to those predicted by DFT calculations. This study not only represents the first example of a quantitative assessment of the XANES spectrum of a dinuclear metal complex to extract transient structural information but also will lead to many future studies in transient structures of multi transition metal complexes commonly used in solar fuel production to perform redox functions as photocatalysts.

Experimental Section

Materials. The starting materials K₂PtCl₄, 2-phenylpyridine, 2,2,6,6-tetramethyl-3,5-heptanedione, and hydrazine were purchased from Aldrich and used as received. [Pt(ppy)μ-Cl]₂ and 3,5-di-*tert*-butylpyrazole (ᵗBu₂pzH) were prepared by literature methods.[38,39] Solvents used for synthesis were reagent grade and used as received.

Synthesis. [Pt(ppy)(μ-ᵗBu₂pz)]₂, (**1**) was prepared by dissolving [Pt(ppy)μ-Cl]₂ (334.5 mg, 0.43 mmol) in 100 mL of 1,2-dichlorobenzene in the presence of 157.6 mg (0.87 mmol) of ᵗBu₂pzH, 350 μL of tributylamine, and 253 mg (0.98 mmol) of AgOTf.[34] When the light-yellow reaction mixture was heated to reflux under argon for 30 min, a white AgCl precipitated formed and the reaction turned deep red in color. The mixture was filtered hot through a bed of alumina in a 60 mL coarse frit to remove 2 equiv of AgCl. After the filtrate was rotary evaporated to near dryness, the orange-red product was isolated by the addition of ethanol and hexanes and subsequent vacuum filtration. Yield 187.2 mg (41%). ¹H NMR (300 MHz, CD₂Cl₂), ppm: 8.25 (d, 2H), 7.61 (t, 2H), 7.40 (d, 2H), 7.23 (d, 2H), 6.85 (m, 4H), 6.28 (s, 2H) 1.32 (s, 36H). MALDI-MS: *m/z* 1057. Anal. Calcd for C₄₄H₅₄N₆Pt₂: C, 49.99; H, 5.15; N, 7.95. Found: C, 49.66; H, 5.01; N, 7.78.

Single crystals suitable for X-ray diffraction were obtained by slow evaporation of a dichloromethane solution containing [Pt(ppy)(μ-ᵗBu₂pz)]₂. Briefly, the orange-red solid was partially dissolved by warming a dichloromethane mixture to 80 °C and sonicating for ∼30 min in a capped vial. The mixture was then filtered warm and the filtrate placed into a second vial capped with a rubber septum with a 22G needle. The saturated solution was then allowed to slowly evaporate undisturbed at room temperature for several days whereupon suitable crystals grew.

Photophysical Measurements. Static UV−vis absorption spectra were measured with a Hewlett-Packard 8453 diode array spectrophotometer. Uncorrected steady-state luminescence spectra were obtained by a PTI Instruments spectrofluorimeter equipped with a 75 W Xe arc lamp/monochromator excitation source, a R-928 PMT, and single photon counting electronics. This fluorimeter operates under the control of FeliX32 software from PTI. All luminescence samples were prepared with spectroscopic grade toluene in 1 cm² anaerobic quartz cells (Starna Cells), degassed by solvent-saturated high-purity argon for at least 35 min prior to the measurements and maintained under argon atmosphere throughout the experiments. Room temperature photoluminescence quantum yields were determined relative to that of [Ru(bpy)₃]²⁺ in dichloromethane (η_{DCM} = 1.3266, Φ_{em} = 0.029).[40]

The excited-state lifetime of **1** is measured using nanosecond transient absorption spectroscopy with pump pulses obtained from the second harmonic output of a Nd:YLF regenerative amplifier laser (λ = 527 nm, 1 kHz, 0.5 mJ/pulse, and 5 ps pulse duration) and probe pulses provided by a xenon flash lamp. The decay of the difference signal is measured and processed using a PMT detector and oscilloscope. A continuously flowing sample of 0.7 mM solution of **1** in toluene is measured in a 0.5

12782 *J. Phys. Chem. A, Vol. 114, No. 48, 2010*

Lockard et al.

mm thick flow cell. The solution sample reservoir was purged with nitrogen gas for ~30 min prior to the pump−probe measurements to remove dissolved oxygen gas from the sample.

X-ray Transient Absorption Spectroscopy. The XTA experiments at the platinum L_{III}-edge (11.564 keV) were conducted at beamline 11ID-D of the Advanced Photon Source at Argonne National Laboratory. The details of this experiment have been described elsewhere.[6,7,41] Briefly, a laser pulse is used to trigger the photoreaction and is followed by an X-ray pulse after some time delay that probes the intermediates along the reaction pathway. The laser pump pulses were generated from the second harmonic output of a Nd:YLF regenerative amplifier laser (λ = 527 nm, 1 kHz, 0.5 mJ/pulse, and 5 ps fwhm at the sample). More recently, Beamline 11ID-D was upgraded to dual in-line undulator insertion device (APS: 3.3 undulator and 2.3 undulator) beamline and the detection system was also updated accordingly. The experiments were carried out in the 24-bunch mode with 153 ns temporal separation between two consecutive X-ray pulses. The X-ray photon flux at the sample was ~5 × 10^6 photons/pulse and the pulse duration was 80 ps fwhm.

The delay time between the laser pump pulse and the X-ray probe pulse was set to nominally 100 ps with the former preceding the latter. The laser and X-ray beams were overlapped spatially at a continuously flowing stream of 0.7 mM solution of **1** in toluene with ~0.5 mm thickness. The solution sample reservoir was continuously purged with nitrogen gas for ~30 min prior to exposure to either laser or X-ray irradiation and throughout the entire duration of the experiment to remove dissolved oxygen gas from the sample. XTA spectra were collected using fluorescence detection at the right angle from the incident X-ray beam. Two X-ray fluorescence detectors consisting of fast plastic scintillator coupled PMTs were used, each of which was behind a Zn filter and custom designed soller slits specifically fitted onto the PMT detector to minimize elastic scattering. A third PMT was used to collect elastic scattering signals from the air for bunch-to-bunch normalization of the incoming X-ray intensity. The outputs from PMTs were connected to two fast analyzer cards (Agilent) where signals from almost all pulses in the entire X-ray pulse train were individually digitized. The pulse shape, the signal offset, and the dark counts were recorded, which were used during data acquisition with in situ curve fitting procedure (G. Jennings, unpublished results). This approach has shown significant improvement of signal-to-noise ratio in XTA spectra, especially for those of low concentrations. A photodiode signal from a part of the laser light processed through a constant fraction discriminator is used as a trigger signal for the analyzer cards. The synchronization and time delay adjustments of the trigger and the X-ray pulses were accomplished by a delay generator to adjust the trigger timing. The data acquisition time window for the analyzer cards was 0.9 ms between two consecutive laser pump pulses. Therefore, about 90% of entire X-ray pulse train was digitized. Si(111) crystals were used in the X-ray mono-chromator. XAS spectra used in analyses were collected with total 200 s integration time at each energy point from ac-cumulated 50 scans.

Computational Methods

Density Functional Theory (DFT) Calculations. The computational study was executed using the Gaussian 03 program.[42] The B3LYP functional[43,44] was employed with the 6-31G(d,p) basis set for the nonmetal atoms (hydrogen, carbon, nitrogen), the LANL2DZ effective core potential (ECP), and corresponding basis set functions[45] for platinum atoms. The geometries of the
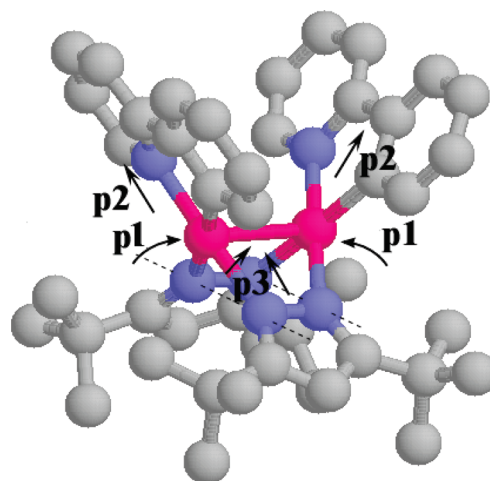

Figure 1. Illustration of the structural parameters used in fitting difference XANES spectra.

singlet ground state and the triplet excited state were calculated using restricted and unrestricted formalisms, respectively. The frequency calculation was performed with the same B3LYP functional and basis sets using the optimized geometry.

XANES Calculations. Refinement of the local structure was performed using multidimensional interpolation approximation (MIA),[36] realized in the FitIt software[46,47] in combination with full multiple scattering (FMS) calculations of XANES using the FDMNES code.[48] We first tested the agreement between the XANES calculation with our method and the experimental results of the ground state with the known structure determined by the X-ray diffraction. The potential energy calculations were performed with the real part of Hedin-Lundqvist exchange and a $5d^8 6s^0$ electronic configuration of Pt. A complex energy with a small imaginary part held constant at 0.2 eV was used to solve FMS equations. The spectral features were broadened using Lorentzian functions with arctangent-type energy-dependent width in order to take the core−hole lifetime and finite mean free path of the photoelectron into account. The center and width of the arctangent function were 40 and 30 eV above the Pt L_{III}-edge, respectively, and maximal broadening width (at high energy) was 15 eV. FMS calculations were performed for a cluster of atoms within 5.5 Å radius centered at the Pt atom.

The refinement of the excited-state structure was performed varying simultaneously the percentage of excited state and structural parameters. The discrepancy between the experimental and theoretical results was minimized in the difference of the photoexcited and the ground state spectra using the formula

$$\min\left(\frac{1}{E_2 - E_1}\int_{E_1}^{E_2} [(\mu_{exp}^{laser\_on} - \mu_{exp}^{laser\_off}) - Y(\mu_{theor}^{es}(\delta p_1, \delta p_2, \delta p_3) - \mu_{theor}^{gs})]^2 \, dE\right) \quad (1)$$

In this formula, $\mu_{exp}^{laser\_on}$ and $\mu_{exp}^{laser\_off}$ are the experimental absorption coefficients measured with and without the laser pump pulse, respectively, μ_{theor}^{es} and μ_{theor}^{gs} are the theoretically calculated absorption coefficients for the excited and ground states, Y is the fraction of the excited state created by the photoexcitation, and E_1 and E_2 define the energy range of the spectral comparison.

The structural parameters used in the calculations are depicted in Figure 1. Parameter p_1 corresponds to the rotation of planes formed by the ppy ligands and Pt atoms around the axes that
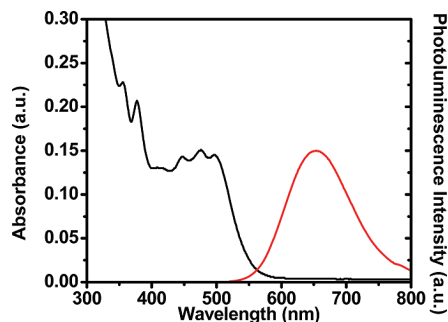
Triplet Excited State Distortions

J. Phys. Chem. A, Vol. 114, No. 48, 2010 **12783**

Figure 2. Steady-state absorption (black) and photoluminescence (red) spectra of [Pt(ppy)(μ-^{t}Bu$_2$pz)]$_2$ (**1**) in toluene.

intersect N atoms of opposite bridging pyrazolate ligands. Variation of this parameter leads to the contraction of Pt−Pt distance, but Pt atoms remain in the plane of ligands. Parameter p_2 corresponds to the rigid shift of the ppy ligands with simultaneous increase of both Pt−C and Pt−N distances while p_3 is the rigid shift of the bridging pyrazolate ligands along their symmetry axes, which changes the Pt−N(bridge) bond lengths. Four structural models were tested, each of which had a shortened Pt−Pt distance compared to that of the ground state while the pyrazolate bridge and ppy ligands were displaced as rigid groups in different directions as shown by arrows in Figure 1. The experimentally observed spectral differences could only be reproduced by a model with simultaneous contractions of Pt−N distances on the pyrazolate bridge and expansions of Pt−C(N) distances of ppy ligands. For this model, distances were varied within the following limits:

p_1 (Pt−Pt distance) 2.67−2.97 Å
p_2 (Pt−C/N(ppy ligand)) 2.00−2.08 Å
p_3 (Pt−N(pyrazolate bridge ligand)) 1.95−2.07 Å

The MIA method allowed us to minimize the number of required full multiple scattering calculations of XANES spectra. On the basis of a few full multiple scattering calculations for different sets of structural parameters (that are called interpolation nodes) we construct the interpolation polynomial that allows us to make accurate prediction of XANES for any other set of parameters within selected limits of variation. We have found that the following interpolation polynomial with energy-dependent coefficients is sufficient to interpolate the spectrum

$$\mu(E, p_1 + \delta p_1, p_2 + \delta p_2, p_3 + \delta p_3) = \mu(E, p_1, p_2, p_3) +$$
$$\sum_{i=1}^{3} A_i(E)\delta p_i + \sum_{\substack{i,j=1 \\ i \neq j}}^{3} B_{ij}(E)\delta p_i \delta p_j + C(E)\delta p_1 \delta p_2 \delta p_3 \quad (2)$$

Thus only eight full multiple scattering calculations are necessary for the refinement of structural parameters for the excited state structure.

Results

Electronic Spectroscopy. The absorption and emission spectra of dilute [Pt(ppy)(μ-^{t}Bu$_2$pz)]$_2$ (**1**) solutions in toluene are displayed in Figure 2. The lowest energy absorption band consists of three peak maxima at 447, 475, and 497 nm assigned to a dinuclear metal−metal-to-ligand charge transfer (MMLCT) from the dσ* orbital derived from σ-orbital interactions between the two Pt metal centers to the π orbital on one of the ppy ligands.[17] The emission is broad and featureless with a significant Stokes shift (peak maximum at 653 nm) and is characteristic
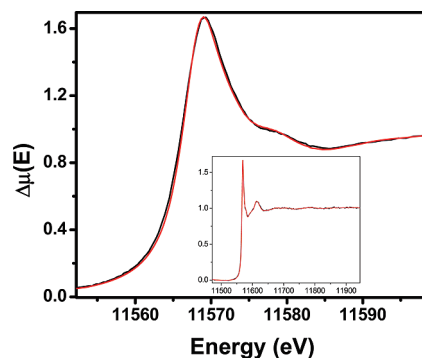

Figure 3. Laser pump off (red line) versus laser pump on (black trace) XANES spectra of **1** in toluene. Inset: Full XAFS spectra.
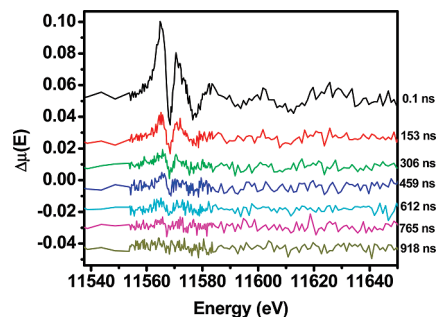

Figure 4. XTA difference spectra (laser pump on − laser pump off) at 0.1, 153, 306, 459, 612, 765, and 918 ns time delays using sequential X-ray pulses in 24 bunch mode. Baselines are offset vertically for ease in viewing.

of triplet state phosphorescence from an excited state with MMLCT parentage ($^3\pi$* → σ*). The emission quantum yield was measured to be 0.032 in argon-saturated toluene solution. The triplet excited state lifetime is measured to be 0.9 μs by optical transient absorption spectroscopy using the same laser excitation source and nearly identical experimental conditions as used for the X-ray experiments (sealed sample reservoir subject to continuous purging with nitrogen gas). The triplet excited state is prone to singlet oxygen quenching as evidenced by an order of magnitude reduction in triplet state lifetime when oxygen is present in solution.

X-ray Transient Absorption Spectroscopy. The transient X-ray absorption spectra obtained for **1** in toluene are shown in Figure 3. The differences between spectra obtained using laser-synched ("laser pump-on") and nonsynched ("laser pump-off") X-ray probe pulses occur in the XANES region and are highlighted in the main graph along with the full XAFS spectra (inset of Figure 3). Several difference spectra ("laser pump on" − "laser pump off") were obtained using sequential X-ray probe pulses between 0 and 1 μs time delay from the laser pump pulse (Figure 4). The oscillatory features in these difference spectra vanish within ∼1 μs after the laser excitation, which match the lifetime of the triplet state with a lifetime of 0.9 μs.

XANES Calculations. The procedures based on full multiple scattering calculations and the MIA method as described in the computational methods section were used to fit the experimental difference XANES spectra. The ground-state XANES spectrum, shown in Figure 5, was calculated using the atomic coordinates derived from the crystal structure of **1** and the nonstructural parameters described above. The difference spectrum obtained at nominal delay time of 100 ps was fit by simultaneously varying the fraction of excited state along with structural parameters defined in Figure 1 which allowed the Pt−Pt, Pt−C, and P−N distances to vary. The resulting best-fit is illustrated
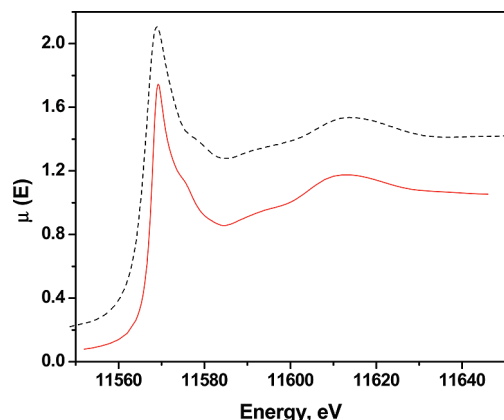
Figure 5. Comparison of experimental (black dashed trace) and theoretical (red solid trace) XANES spectra for the ground state of **1**.
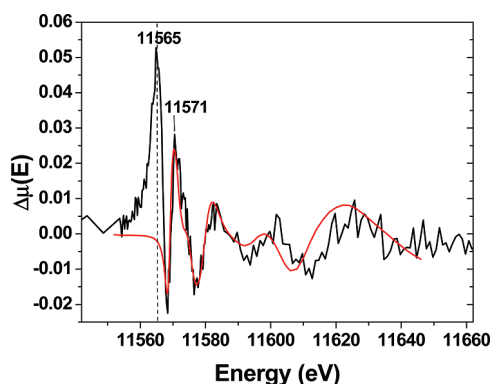

Figure 6. Experimental difference between laser-on and laser-off spectra (black dashed line) and best-fit theoretical spectrum (solid red line).

in Figure 6. The first positive sharp feature at 11565 eV in the experimental difference spectrum arises from the electronic transition from 2p to a 5d orbital that is vacated by the laser pump pulse excitation. This peak is not reproduced in the theoretical simulations and was excluded from the fitting procedure since all nonstructural parameters (including Fermi energy) were exactly the same for the ground and photoexcited states. This constraint on the nonstructural parameters is required for a stable fitting procedure and has been successfully applied previously.[37] Thus only those features that originate from the changes of the local structure were fitted using the MIA approach.

The atomic distances derived from the structural refinement used to fit the difference spectrum are listed in Table 1 and compared to those obtained from the ground-state crystal structural and the DFT calculated geometries for the S_0 and T_1 states. In the present case, there is quite good agreement between the DFT-calculated Pt−Pt distance in the S_0 state and that measured in the X-ray crystal structure. In fact, the relative distance correlation between theory and experiment presented here (0.05 Å) is more closely matched with respect to that previously reported for the related [Pt(F$_2$ppy)(μ-^{t}Bu$_2$pz)]$_2$ complex (0.1 Å).[33] According to the DFT calculations, the
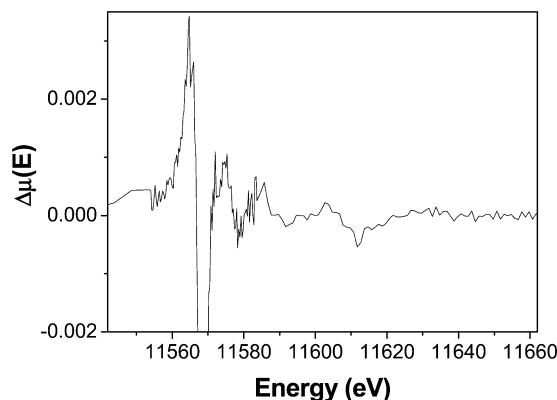

Figure 7. Difference between additionally broadened (Gaussian 0.5 eV) and initial (nonbroadened) ground-state spectra.

metal−metal distance in the lowest triplet excited state in **1** is predicted to contract by 0.3 Å. This is essentially identical to that calculated for the same orbital configuration in the [Pt(F$_2$ppy)(μ-^{t}Bu$_2$pz)]$_2$ complex (0.29 Å).[33] In essence, the DFT calculations are consistent with frontier MO picture rendering an excited state that can be considered partially bonding from a metal−metal standpoint.

Discussion

While structural changes that occur upon population of the ^{3}MMLCT excited state of **1** can be extracted from the oscillations observed in the XANES difference spectra, other possible mechanisms that may produce the similar difference spectra need to be considered. In particular, heating due to laser excitation can raise the temperature of the sample, causing the Debye−Weller factors to increase.[49−51] This would effectively broaden the electronic transition at the Pt L$_{III}$-edge region featuring the 2p to 5d transition and result in the amplitude attenuation of the XAFS oscillatory features. This thermal effect can be demonstrated by the simulated difference spectrum in Figure 7, which is derived by subtracting the experimental ground state (laser off) spectrum from an artificially broadened (Gaussian 0.5 eV) version of itself. The simulated broadened spectrum exhibits broader transition peaks and reduced oscillatory amplitude compared to the original experimental ground-state spectrum. At first glance, the spectrum in Figure 7 is reminiscent of what we observed in the experiments shown in Figure 4.

However, if the spectral changes are due to a mere heating process, their decay kinetics will differ from that of the triplet excited state, because the time constants for solvent thermodiffusivity and excited state decay are on very different time scales. Because the time decay of the oscillations in the difference spectrum follows that of the triplet excited state, which has a time constant of ∼1 μs, these oscillatory features are clearly only associated with the excited-state population. Hence, we can rule out the thermal effect as the cause of the difference spectra shown in Figure 4.

Another possible cause of the oscillatory feature broadening comes from increased molecular structural diversity in the ground state upon deactivation from the triplet excited state. A

TABLE 1: Comparison of Structural Parameters for S_0 and T_1 States Derived from the DFT Calculations, X-ray Diffraction, and XTA with the Best Fit under a Certain Value of Y (the fraction of the excited state)

bond partners	S_0 (DFT)	T_1 (DFT)	S_0 (experimental crystal structure)	T_1 $Y = 45\%/30\%$ (XANES best fit)
Pt−Pt	3.02	2.72	2.97	2.77/2.74
Pt−N$_1$, Pt−N$_2$ (pyrazolate)	2.07, 2.23	2.08, 2.23	2.07	1.98/1.95
Pt−C, Pt−N (ppy)	2.06, 2.00	2.04, 2.01	2.00	2.03/2.06

Triplet Excited State Distortions

J. Phys. Chem. A, Vol. 114, No. 48, 2010 **12785**

significant displacement of the triplet excited state surface along the Pt−Pt stretch or other vibrational coordinates relative to that of the ground state would effectively lead to the initial population of hot vibrational states with a wider degree of structural variation upon vibrational relaxation or vibrational cooling. From a kinetics point of view however, capturing these hot vibrational states with the X-ray probe is statistically unrealistic since vibrational cooling typically occurs on a ∼10 ps time scale while the total lifetime of the T_1 state is nearly 1 μs. In other words, the average duration time that the excited state molecules spend in the "hot" vibrational levels is 5 orders of magnitude less than the time spent in the thermally equilibrated vibrationally relaxed excited T_1 state. The resulting transient population difference would not be observable from these experiments.

A more feasible broadening mechanism would involve a complicated triplet excited state manifold with greater structural variation in the excited state than in the ground state. This mechanism can be realized if the ^{3}MMLCT state of **1** were coupled with another triplet state similar in energy, such as a ligand-centered (LC) state. However, our DFT calculations indicate that for the *t*-Bu substituted version of these Pt dimers, the LC triplet state is significantly higher in energy than the ^{3}MMLCT state, which rules out significant coupling between the two states. Thus, this mechanism is also considered invalid.

With these broadening mechanisms discounted, the oscillations observed in the difference spectra are primarily attributed to a combination of electronic and structural changes accompanying the excited state population. The first positive oscillatory feature in these XANES difference spectra results from a new electronic transition of the laser-on spectrum, which is consistent with the $2p \rightarrow 5d$ transition expected due to the $d_{\sigma*}$ orbital vacancy created in the excited-state electron configuration. The remaining part of the oscillations is attributed to the molecular geometry changes associated with the excited state. The average nearest neighbor bond lengths of the ground and excited states structures are extracted from the fit to this part of the difference spectrum. The fraction of excited state Y is usually determined by comparing the ground-state optical density with that of the ground-state bleach signal using transient absorption methods. However, in the case of **1**, a broad positive transient absorption signal that extends throughout the visible wavelength range nearly cancels out the ground-state bleach and prevents an accurate excited state fraction measurement. For this reason the excited state fraction Y is treated as a variable in the fitting routine. The best fits were obtained using $Y = 30−45\%$. The bond lengths derived from the two extremes of this range are reported in Table 1. The small variations in bond lengths imply that the fitting is relatively insensitive to Y. The distances obtained from the fits indicate a Pt−Pt bond length decrease in the excited state by 0.20−0.23 Å, which agrees with the simple MO prediction described above as well as the DFT calculations. The fitting also reveals a reduction in bond length between the platinum and bridging ligands by 0.1−0.15 Å, despite the prediction of minimal change in these distances by DFT. This discrepancy may originate from the solvation of the molecule which was excluded in the DFT calculations. Given the respectable fit using different ground- and excited-state molecular structures and the unlikelihood of contributions from other broadening mechanisms, the oscillations in the observed difference spectra are assigned to the change in equilibrium geometry associated with the triplet excited state. The weak signal at higher energies contributes to the difficulty in fitting this region of the spectrum. In other words the changes in the
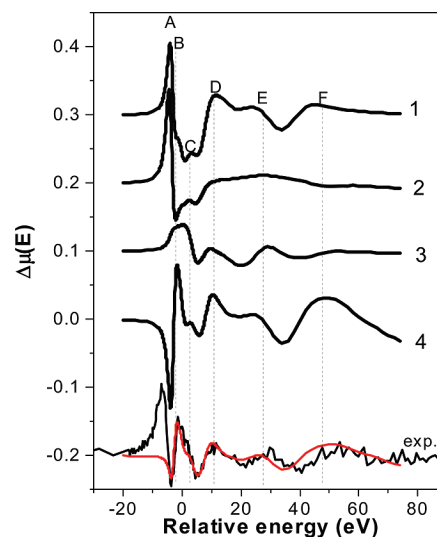

Figure 8. Calculated difference XANES spectra of the complex (μ_{theor}^{es} and μ_{theor}^{gs}) from the four structural models: (1) contraction of Pt−Pt distance by 0.3 Å (parameter p1 only); (2) expansion of Pt−N/C(ppy) distance by 0.08 Å and contraction of Pt−Pt distance by 0.3 Å; (3) expansion of Pt−N/C(ppy) distance by 0.08 Å and contraction of Pt−N(bridge) distance by 0.09 Å; (4) contraction of Pt−Pt distance by 0.3 Å and contraction of Pt−N(bridge) distance by 0.09 Å. Curve 2 is divided by 4 to match the scale of other graphs; spectra are also shifted vertically. For comparison, the experimental data and the best fit are also shown in the bottom.

EXAFS region produced by the structural changes between the ground and excited state of **1** are too small to accurately model.

In order to demonstrate the sensitivity of the XANES spectrum to the structural variations, we have calculated difference spectra for four different structural models of photoexcited complexes shown in Figure 8. In the first model where only the contraction of the Pt−Pt distance is applied, the calculated spectrum (curve 1) has a negative signal at feature B whereas the analogous feature in the experimental difference spectrum is positive. Also, while features D, E, and F of the difference spectrum derived from this model resemble those observed experimentally, the intensity of feature C is not reproduced. In the second model, where increases of the Pt to the ppy ligand distances are applied in addition to the Pt−Pt distance contraction from model 1, the calculated spectrum produces an energy shift that manifests itself as a huge positive peak (labeled A in curve 2) that overwhelms the effect of Pt−Pt bond contraction in the white-line energy region, which differs significantly from the experimental difference spectra. This huge peak can be partially attenuated in the third model by the contraction of Pt−N (pyrazolate) bonds (curve 3) without the contraction of Pt−Pt distance, but the overall shape of the spectrum significantly deviates from the experimental difference spectrum. Hence, reasonable results can only be achieved if the Pt−Pt distances and Pt−N (pyrazolate) bonds are simultaneously contracted (curve 4). Finally, the best fit to the experimental spectrum using this model is achieved with the structural parameters in Table 1.

The combined experimental and theoretical approach in the above analyses have confirmed the Pt−Pt distance contraction in the triplet state of **1**, which otherwise is missed using conventional XAFS data analysis. The difficulty encountered here reveals challenges in extracting transient metal−metal distances from nonbonding or weak-bonding systems. In particular, **1** has a "hinged" motif, and the Pt−Pt distance can be perturbed by multiple rocking, twisting, and bending motions

via different vibrational modes at very low frequencies (i.e., <100 cm^{-1}) due to the large reduced masses associated with the corresponding harmonic oscillators. Hence the value of the Debye−Weller factor associated with the Pt−Pt distance, σ^2(Pt−Pt), in the conventional XAFS equation[52] would be large and dependent on multidimensional nuclear coordinates. In addition, the smaller energy gaps between the low frequency Pt−Pt stretching vibrational levels (i.e., 100 cm^{-1} = 0.0124 eV)[32] enable significant populations of higher vibrational levels at room temperature (i.e., kT = 0.0256 eV) based on the Boltzmann distribution, adding uncertainties in the Pt−Pt distance. In the XTA study by van der Veen et al. on the excited-state structure of Pt$_2$(pop)$_4$ where the Pt−Pt is held more rigidly than in **1** by four bridges, the Pt−Pt distance in the excited triplet state was also extracted via extensive mapping of multiple coordinates in relatively wide ranges rather than by conventional XAFS data fitting. Both cases indicate the challenges in fitting such a transient structures using the conventional XAFS analysis routine.

We have demonstrated the capabilities and challenges in extracting metal−metal distances in nonbonding and weak-bonding a transition metal complex by the XTA and MIA methods. The results will have an important impact in capturing transient structures of many photocatalytic transition metal complexes in solar fuel production since the multimetal clusters are common motifs in these catalysts intended to facilitate multiple electron transfer reactions from sequential single photon events.

Conclusion

Solution-based XTA experiments combined with the multidimensional interpolation approximation were used to extract molecular level structural changes of [Pt(ppy)(μ-^{t}Bu$_2$pz)]$_2$ in toluene accompanying an electronic transition induced by the laser excitation. These results on the structural changes are supported by the theoretical calculations wherein the d^8−d^8 transition metal dimers possessing nonbonding dσ* ground states become partially bonding in their excited states due to the depletion of this formally antibonding molecular orbital. Fitting the XTA difference spectra from full multiple scattering calculations with the experimental results revealed a Pt−Pt bond compression of approximately 0.2 Å in the triplet excited state of [Pt(ppy)(μ-^{t}Bu$_2$pz)]$_2$, consistent with transient production of a metal−metal bonding interaction. This Pt−Pt bond compression correlated well with those predicted by DFT calculations performed on the lowest triplet excited state of **1**. The application of the multidimensional interpolation approximation approach to fitting the difference XTA spectrum is an alternative way for extracting structural parameters compared to conventional XAFS data analysis. In a more general sense, current solution-based XTA measurements using the consecutive pulse train are capable of unraveling structural rearrangements accompanying light stimulation of molecular species on different time scales from 100 ps to longer. With the X-ray free electron lasers being operational and constructed around the world, we expect that direct structural snapshots or even molecular movies can be made in not so distant future in our future studies.

References and Notes

(1) Butler, J. M.; George, M. W.; Schoonover, J. R.; Dattelbaum, D. M.; Meyer, T. J. *Coord. Chem. Rev.* **2007**, *251*, 492–514.
(2) Browne, W. R.; McGarvey, J. J. *Coord. Chem. Rev.* **2007**, *251*, 454–473.
(3) Nibbering, E. T. J.; Fidder, H.; Pines, E. *Annu. Rev. Phys. Chem.* **2005**, *56*, 337–367.
(4) Hunt, N. T. *Chem. Soc. Rev.* **2009**, *38*, 1837–1848.
(5) Kim, Y. S.; Hochstrasser, R. M. *J. Phys. Chem. B* **2009**, *113*, 8231–8251.
(6) Chen, L. X. *Angew. Chem., Int. Ed.* **2004**, *43*, 2886–2905.
(7) Chen, L. X. *Annu. Rev. Phys. Chem.* **2005**, *56*, 221–254.
(8) Chen, L. X.; Jager, W. J. H.; Jennings, G.; Gosztola, D. J.; Munkholm, A.; Hessler, J. P. *Science* **2001**, *292*, 262–264.
(9) Chen, L. X.; Shaw, G. B.; Liu, T.; Jennings, G.; Attenkofer, K. *Chem. Phys.* **2004**, *299*, 215–223.
(10) Chen, L. X.; Zhang, X. Y.; Wasinger, E. C.; Attenkofer, K.; Jennings, G.; Muresan, A. Z.; Lindsey, J. S. *J. Am. Chem. Soc.* **2007**, *129*, 9616.
(11) Chen, L. X.; Shaw, G. B.; Novozhilova, I.; Liu, T.; Jennings, G.; Attenkofer, K.; Meyer, G. J.; Coppens, P. *J. Am. Chem. Soc.* **2003**, *125*, 7022–7034.
(12) Bressler, C.; Milne, C.; Pham, V. T.; ElNahhas, A.; van der Veen, R. M.; Gawelda, W.; Johnson, S.; Beaud, P.; Grolimund, D.; Kaiser, M.; Borca, C. N.; Ingold, G.; Abela, R.; Chergui, M. *Science* **2009**, *323*, 489–492.
(13) Gawelda, W.; Cannizzo, A.; Pham, V. T.; El Nahhas, A.; Milne, C. J.; van der Veen, R.; Bressler, C.; Chergui, M. In *Fall Meeting of the Swiss-Chemical-Society*; Swiss Chemical Society: Zurich, Switzerland, 2006; Vol. 61, pp 179−183.
(14) Esswein, A. J.; Veige, A. S.; Nocera, D. G. *J. Am. Chem. Soc.* **2005**, *127*, 16641–16651.
(15) Heyduk, A. F.; Nocera, D. G. *Science* **2001**, *293*, 1639–1641.
(16) Ma, B. W.; Djurovich, P. I.; Garon, S.; Alleyne, B.; Thompson, M. E. *Adv. Funct. Mater.* **2006**, *16*, 2438–2446.
(17) Ma, B. W.; Li, J.; Djurovich, P. I.; Yousufuddin, M.; Bau, R.; Thompson, M. E. *J. Am. Chem. Soc.* **2005**, *127*, 28–29.
(18) Fox, L. S.; Marshall, J. L.; Gray, H. B. *J. Am. Chem. Soc.* **1987**, *109*, 6901–6902.
(19) Mccleskey, T. M.; Winkler, J. R.; Gray, H. B. *Inorg. Chim. Acta* **1994**, *225*, 319–322.
(20) Fox, L. S.; Kozik, M.; Winkler, J. R.; Gray, H. B. *Science* **1990**, *247*, 1069–1071.
(21) Miskowski, V. M.; Rice, S. F.; Gray, H. B.; Dallinger, R. F.; Milder, S. J.; Hill, M. G.; Exstrom, C. L.; Mann, K. R. *Inorg. Chem.* **1994**, *33*, 2799–2807.
(22) Miskowski, V. M.; Rice, S. F.; Gray, H. B.; Milder, S. J. *J. Phys. Chem.* **1993**, *97*, 4277–4283.
(23) Milder, S. J.; Brunschwig, B. S. *J. Phys. Chem.* **1992**, *96*, 2189–2196.
(24) Leung, K. H.; Phillips, D. L.; Che, C. M.; Miskowski, V. M. *J. Raman Spectrosc.* **1999**, *30*, 987–993.
(25) Clodfelter, S. A.; Doede, T. M.; Brennan, B. A.; Nagle, J. K.; Bender, D. P.; Turner, W. A.; Lapunzina, P. M. *J. Am. Chem. Soc.* **1994**, *116*, 11379–11386.
(26) Che, C. M.; Butler, L. G.; Gray, H. B.; Crooks, R. M.; Woodruff, W. H. *J. Am. Chem. Soc.* **1983**, *105*, 5492–5494.
(27) Striplin, D. R.; Crosby, G. A. *J. Phys. Chem.* **1995**, *99*, 7977–7984.
(28) Rice, S. F.; Gray, H. B. *J. Am. Chem. Soc.* **1983**, *105*, 4571–4575.
(29) Thiel, D. J.; Livins, P.; Stern, E. A.; Lewis, A. *Nature* **1993**, *362*, 40–43.
(30) Kim, C. D.; Pillet, S.; Wu, G.; Fullagar, W. K.; Coppens, P. *Acta Crystallogr., Sect. A* **2002**, *58*, 133–137.
(31) van der Veen, R. M.; Milne, C. J.; El Nahhas, A.; Lima, F. A.; Pham, V. T.; Best, J.; Weinstein, J. A.; Borca, C. N.; Abela, R.; Bressler, C.; Chergui, M. *Angew. Chem., Int. Ed.* **2009**, *48*, 2711–2714.
(32) Christensen, M.; Haldrup, K.; Bechgaard, K.; Feidenhans'l, R.; Kong, Q. Y.; Cammarata, M.; Lo Russo, M.; Wulff, M.; Harrit, N.; Nielsen, M. M. *J. Am. Chem. Soc.* **2009**, *131*, 502–508.
(33) Saito, K.; Nakao, Y.; Sakaki, S. *Inorg. Chem.* **2008**, *47*, 4329–4337.

Triplet Excited State Distortions

J. Phys. Chem. A, Vol. 114, No. 48, 2010 **12787**

(34) Rachford, A. A.; Castellano, F. N. *Inorg. Chem.* **2009**, *48*, 10865–10867.

(35) van der Veen, R. M.; Kas, J. J.; Milne, C. J.; Pham, V. T.; El Nahhas, A.; Lima, F. A.; Vithanage, D. A.; Rehr, J. J.; Abela, R.; Chergui, M. *Phys. Chem. Chem. Phys.* **2010**, *12*, 5551–5561.

(36) Smolentsev, G.; Soldatov, A. *Journal of Synchrotron Radiation* **2006**, *13*, 19–29.

(37) Smolentsev, G.; Soldatov, A. V.; Chen, L. X. *J. Phys. Chem. A* **2008**, *112*, 5363–5367.

(38) Brooks, J.; Babayan, Y.; Lamansky, S.; Djurovich, P. I.; Tsyba, I.; Bau, R.; Thompson, M. E. *Inorg. Chem.* **2002**, *41*, 3055–3066.

(39) Wang, Z. X.; Qin, H. L. *Green Chem.* **2004**, *6*, 90–92.

(40) Caspar, J. V.; Meyer, T. J. *J. Am. Chem. Soc.* **1983**, *105*, 5583–5590.

(41) Jennings, G.; Jaeger, W. J. H.; Chen, L. X. *Rev. Sci. Instrum.* **2002**, *72*, 362–368.

(42) Frisch, M. J.; Trucks, G. W.; Schlegel, H. B.; Scuseria, G. E.; Robb, M. A.; Cheeseman, J. R.; Montgomery, J. A., Jr.; vreven, T.; Kudin, K. N.; Burant, J. C.; Millam, J. M.; Ivengar, S. S.; Tomasi, J.; Barone, V.; Mennucci, B.; Cossi, M.; Scalmani, G.; Rega, N.; Petersson, G. A.; Nakatsuji, H.; Hada, M.; Ehara, M.; Toyota, K.; Fukuda, R.; Hasegawa, J.; Ishida, M.; Nakajima, T.; Honda, Y.; Kitao, O.; Nakai, H.; Klene, M.; Li, X.; Knox, J. E.; Hratchian, H. P.; Cross, J. B.; Bakken, V.; Adamo, C.; Jaramillo, J.; Gomperts, R.; Stratmann, R. E.; Yazyev, O.; Austin, A. J.; Cammi, r.; Pomellli, C.; Ochterski, J. W.; Ayala, P. Y.; Morouma, K.; Voth, G. A.; Salvador, P.; Dannenberg, J. J.; Zakrzewski, V. G.; Dapprich, S.; Daniels, A. D.; Strain, M. C.; Farkas, O.; Malick, D. K.; Rabuck, A. D.; Raghavachari, K.; Foresman, J. B.; Ortiz, J. V.; Cui, Q.; Baboul, A. G.; Clifford, S.; Cioslowski, J.; Stefanov, B. B.; Liu, G.; Liashenko, A.; Piskorz, P.; Komaromi, I.; Martin, R. L.; Fox, D. J.; Keith, T.; Al-Laham, M. A.; Peng, C. Y.; Nanayakkara, A.; Challacombe, M.; Gill, P. M. W.; Johnson, B.; Chen, W.; Wong, M. W.; Gonzalez, C.; Pople, J. A. *Gaussian 03*; Gaussian, Inc.: Wallingford, CT, 2004.

(43) Becke, A. D. *J. Chem. Phys.* **1993**, *98*, 5648–5652.

(44) Lee, C.; Yang, W.; Parr, R. G. *Phys. Rev. B* **1988**, *37*, 785–789.

(45) Hay, P. J.; Wadt, W. R. *J. Chem. Phys.* **1985**, *82*, 299–310.

(46) Smolentsev, G.; Soldatov, A. V. *Comput. Mater. Sci.* **2007**, *39*, 569–574.

(47) www.nano.sfedu.ru/fitit.html.

(48) Joly, Y. *Phys. Rev. B* **2001**, *63*, 125120.

(49) Sayers, D. E.; Stern, E. A.; Lytle, F. *Phys. Rev. Lett.* **1971**, *27*, 1204–1207.

(50) Lytle, F. W.; Sayers, D. E.; Stern, E. A. *Phys. Rev. B* **1975**, *11*, 4825–4835.

(51) Stern, E. A.; Sayers, D. E.; Lytle, F. W. *Phys. Rev. B* **1975**, *11*, 4836–4846.

(52) Bunker, G. *Introduction to XAFS: A Practical Guide to X-ray Absorption Fine Structure Spectroscopy*; Cambridge University Press: Cambridge and New York, 2010.

JP1088299